Object-Based Validation of a Sentinel-2 Burned Area Product Using Ground-Based Burn Polygons

Luca Pulvirenti, *Member, IEEE*, Giuseppe Squicciarino, Dario Negro, and Silvia Puca

***Abstract*—An object-based validation of a country (Italy) level burned area product is proposed, to assess not only the thematic accuracy, but also the geometric accuracy. The product was derived from Sentinel-2 data by using an algorithm, already published in the literature, which applies image segmentation. Ground-based burn polygons, representing the official burned area data for Italy, were used, as reference, to assess the product. The validation was performed by implementing a set of accuracy metrics to quantify the similarity between reference objects and mapped objects, the object-based thematic accuracy, and the global quality of the segmentation. The challenges in performing the object-based validation, mainly related to the absence of a one-to-one relationship between a reference object and a mapped one, are discussed and the strengths and weaknesses of the considered burned area product are highlighted. Results showed that the product was characterized by a good geometric accuracy even if the number of false positives represented a critical point. Although a specific product was used, the proposed validation method can be in principle applied to any burned area data derived from satellite images. To point out this characteristic, an experiment on another product was performed too.**

***Index Terms*—Burned area (BA) mapping, fires, Italy, per-polygon approach, Sentinel-2, validation.**

I. Introduction

THE use of coarse resolution satellite data for burned area (BA) mapping is well consolidated. At present, the 500 m moderate resolution imaging spectroradiometer (MODIS) product [1] and the 250 m MODIS Fire_cci version 5.1 product [2], developed as part of the climate change initiative (CCI), provide the scientific community with timely data regarding the extent of the of the areas affected by fire. However, there is also an increasing interest in the use of moderate resolution data for the generation of BA products. Previous investigations demonstrated that both Landsat and Sentinel-2 (S2) data are able to map small and/or fragmented BAs [3], while coarse resolution data have difficulties in detecting small fires (< 100 ha) [4].

Several country-to-continental level products were generated using Landsat and/or S2 data. In the framework of the monitoring trends in burn severity project, a systematic BA mapping in the United States was performed using Landsat data [5]. A method to map 30 m burned areas at regional scale through a combination of Landsat data and MODIS active fire detections was developed in [6]. An operational BA mapping in Queensland was proposed in [7] using Landsat reflectance time series. An approach for estimating BA in Mato Grosso (Brazil) was designed in [8]. An algorithm to identify BAs in the conterminous United States using Landsat images was presented in [9] and updated in [10]. A combination of Landsat and S2 data for BA mapping in Southern Africa was performed in [3]. The Small Fire Database Fire_cci v1.1 (FireCCISFD11) product, which included BA detected over the Sub-Saharan Africa from S2 and MODIS active fire detections, was presented in [11], while its evolution was described in [12].

To validate global resolution products, BA maps derived from higher spatial resolution satellite images are commonly used as reference data (e.g., [13], [14]), in agreement with the Committee on Earth Observation Satellites (CEOS) protocol [15]. Applying the same approach to assess products generated using moderate resolution data may be critical. In this case, freely available images with higher resolution are difficult to find. Planet data were used as reference in [3] and [16]. In [11], Landsat data were exploited to validate S2-derived BAs, while in [4] two different teams generated S2-derived BA maps.

Ground measurements represent independent reference data that can be profitably exploited to validate moderate resolution data, because they are usually derived from global positioning system (GPS) devices with metric accuracy. While it is unrealistic to collect ground data at global or continental scale, in principle it is possible to do it at smaller (e.g., national) scale. In Italy, ground surveys are performed by the authorities that are officially in charge of mapping the areas affected by fire. Burn polygons derived from these surveys represent the official BA data for Italy. Then, end users of BA products derived from satellite remote sensing images (the Italian Department of Civil Protection – DCP and regional authorities) usually request to assess these products versus the official data.

In the literature, the result of the comparison of a BA product with reference data is generally expressed in terms of confusion matrix, which provides a foundation to describe general classification accuracy [17]. From the confusion matrix, parameters like

Manuscript received 31 May 2023; revised 14 August 2023; accepted 8 September 2023. Date of publication 18 September 2023; date of current version 13 October 2023. This work was supported by the Italian Department of Civil Protection, Presidency of the Council of Ministers, through the convention between Department of Civil Protection and CIMA Research Foundation, for the development of knowledge, methodologies, technologies, and training, useful for the implementation of national systems of monitoring, prevention, and surveillance. *(Corresponding author: Luca Pulvirenti.)*

Luca Pulvirenti and Giuseppe Squicciarino are with the CIMA Research Foundation, I-17100 Savona, Italy (e-mail: luca.pulvirenti@cimafoundation.org; giuseppe.squicciarino@cimafoundation.org).

Dario Negro and Silvia Puca are with the Italian Department of Civil Protection, Presidency of the Council of Ministers, I-00189 Rome, Italy (e-mail: dario.negro@protezionecivile.it; silvia.puca@protezionecivile.it).

Digital Object Identifier 10.1109/JSTARS.2023.3316303

overall accuracy, omission and commission errors (e.g., [3], [18], [19]), as well as the Dice coefficient that synthetically combines omission and commission (e.g., [13], [16], [19]) are derived.

A burn polygon (or, more generally, an actual BA) can be assumed as an object on the ground with its own location, extent and shape. Quantifying the ability of a BA product derived from remote sensing data to retrieve location, extent and shape of an actual BA represents an important information for any stakeholder. In fact, BA data may be used to generate a fire cadaster (as done in Italy), which, on its turn, may be used to establish time constraints on the land use of the areas affected by fire. For instance, in Italy it is forbidden to change the use of an area affected by fire for at least 15 years. In [20], it is suggested that if the map to be assessed is a polygon map, then the accuracy assessment sample units should also be polygons. In [21], it is pointed out that the shape and size of individual fires represent an important topic regarding ecology and fire succession, as well as landscape management and fire spread rate. Moreover, although on most wildfires there are islands of unburned vegetation scattered throughout the burned area, these areas are often not mapped through ground surveys, because of safety concerns or the impossibility of delineating numerous small patches on the ground [22]. This affects the result of a per-pixel approach to accuracy assessment based on the confusion matrix, if ground-based burn polygons are used as reference data. Thereby the idea that a per-polygon approach to accuracy assessment, that is, an object-based validation, can complement a per-pixel approach based on the confusion matrix.

Formally, an object-based validation gives information on if and how well a mapped object M spatially matches a reference object R [23]. To perform this kind of validation, a BA mapping algorithm applying an object-based approach is particularly suitable. With respect to coarse resolution sensors, higher resolution ones increase the within-class spectral variability, thus decreasing the potential accuracy of a purely pixel-based approach to classification [24]. This highlights the utility of using, for BA mapping from moderate resolution data, an algorithm that groups multiple neighboring pixels into one object, based on similar spectral characteristics of these pixels. The process of generating objects is known as segmentation [17].

Since 2019, the Italian DCP uses a processor, called AUTOmatic Burned Areas Mapper (AUTOBAM), to map BAs from S2 data in near-real time (NRT). AUTOBAM, implements an algorithm that basically merges pixels to object clusters, thus performing an image segmentation; segments are successively analyzed and classified [25]. AUTOBAM, which works at country level (Italy), has been originally proposed in [26]; its most recent release is described in [27].

While, as mentioned before, the validation of BA products based on a confusion matrix was widely adopted in the literature (e.g., [13], [14], [16], [18]), and was done in [27] for AUTOBAM, the analysis of the match/mismatch between BA objects was rarely performed. In [21], a method for characterizing the accuracy of the shape of coarse resolution BA detections, by comparing them to higher resolution reference BAs, was proposed. In [28], an intercomparison of two global BA products was carried out by analyzing the morphological features of fire patches. A service using not only BA data derived from high-resolution satellites, but also fire perimeter polygons compiled by local authorities was described in [29]; the burn polygons were used to evaluate the detection count in this case. Regarding AUTOBAM, the match/mismatch between BA objects was preliminary assessed in [27], but considering a very limited set of parameters.

This article presents a new method designed to perform an object-based validation of a BA product derived from satellite data using ground-based burn polygons as reference data. The method is based on the analysis of the match/mismatch between mapped BA objects and real-world objects. The analysis is done by computing metrics for assessing individual objects, per class measures and parameters to evaluate the overall quality of the segmentation. In this way, a comprehensive assessment of the strengths and weaknesses of the considered product is provided. To conduct the study, the BA product was generated from S2 data by using AUTOBAM. In addition, to show that the proposed validation procedure can be applied to any product derived from satellite data, an exercise in which the European Forest Fire Information System (EFFIS) product was used instead of the AUTOBAM one was carried out. The critical aspects of an object-based validation of a BA product using ground-based burn polygons, mostly related to the absence of a one-to-one correspondence between a mapped object and a reference object, were also analyzed.

II. Materials and Methods

A. Study Area and Reference Data

The study area was Italy where fires are mostly located in the southern regions and the fire season corresponds to period June 1–September 30. During each fire season, the Carabinieri Command of Units for Forestry, Environmental and Agri-food protection and, for autonomous regions, the regional forestry corps perform a ground survey campaign to map the perimeters of the fires daily notified by the operational rooms (namely the Permanent Unified Operating Centers). The ground measurements are taken using GPS devices with metric accuracy.

Burn polygons derived from the ground measurements, available in vector (shapefile) format, represent the official BA data for the Italian stakeholders as DCP. The shapefile attributes include the information about the extent of each BA (in ha) and the fire date. To carry out the present study, the ground data gathered during the 2021 fire season were used as reference. We focused on 2021, because fires with very different extent broke out during this year and we analyzed the capability of the mapped BAs to retrieve the extent of reference BAs. Although in a Mediterranean environment like Italy fires are usually small [27], [30], in 2021 about 20 fires burned an area larger than 1000 ha.

B. EFFIS Data

As mentioned in the Introduction, besides the AUTOBAM BA product, the EFFIS product was also used to highlight that the proposed validation procedure can be applied to any BA dataset.

The EFFIS product is derived from the daily processing of MODIS data and, since 2018, S2 data. BAs of about 30 ha or larger are mapped, but the product may also include BAs of smaller dimension, which are mapped from S2 imagery. The EFFIS product delineates the extent of forest fire events. It is generated by first applying an unsupervised procedure that uses a combination of band thresholds, ancillary information regarding land cover and active fire detections. Then, fires are verified and corrected through visual interpretation of the MODIS and S2 images [31].

C. Overview of the AUTOBAM Processor

This section summarizes the main characteristics of the AUTOBAM processor. Note that this article does not focus on the description of AUTOBAM, but rather on the methodology to perform an object-based validation of a BA product based on moderate resolution satellite data. The reader is referred to papers [26] and [27] for more details about AUTOBAM.

AUTOBAM is a fully automatic processing chain for NRT BA mapping from S2 data. It systematically downloads and processes all the S2 observations of Italy (cloud cover $<$ 40%). According to the NRT requirement, BA maps are produced within 6–8 h from the time S2 data are available in the Copernicus Open Access Hub.[1] To meet this requirement, AUTOBAM does not take advantage of the temporal persistence of fire effects, which is accounted for in [3] and [4], because it would imply the use of at least two post fire images, resulting in a delay in the estimation of the extent of a BA. Then, AUTOBAM uses pairwise observations to apply a change detection-based approach.

The atmospherically corrected S2 Level-2A (L2A) surface reflectance products, which include a scene classification (SCL) map useful to mask clouds, cloud shadows and water bodies, are used by AUTOBAM to generate the BA maps. From these data, three spectral indices based on near infrared (NIR) and shortwave infrared (SWIR) bands are derived, namely the normalized burn ratio (*NBR*), the normalized burn ratio 2 (*NBR2*) and the mid-infrared burned index (*MIRBI*). *NBR* is based on NIR and long SWIR bands, while *NBR2* and *MIRBI* are based on the short and long SWIR bands. The change detection approach basically compares the values of the indices acquired at current time with the values derived from the most recent cloud-free S2 data.

As schematized in Fig. 1, the BA mapping consists of the following steps:

1) Computation of three bitemporal spectral indices (BTSIs);
2) application of a clustering algorithm to identify a first guess BA;
3) detection of the edges of the first guess BA using the Roberts filter;
4) creation of a buffer zone around the edges;
5) computation, through the Otsu method [32], of a threshold for each BTSI which separates the BA from the unburned area using only the pixels in the buffer;
6) application of a region growing algorithm (RGA).

[1][Online]. Available: https://scihub.copernicus.eu/dhus/#/home

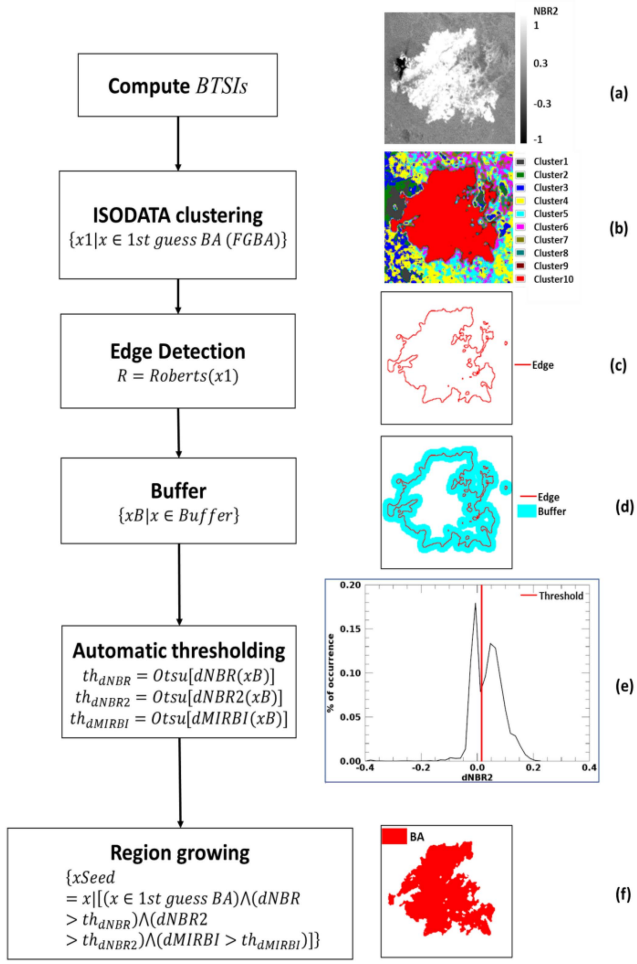

Fig. 1. Flowchart of the BA mapping algorithm implemented in AUTOBAM (x denotes a generic pixel).

Changes are evaluated by computing the following BTSIs:

$$dNBR = NBR\,(t_1) - NBR\,(t_2) \tag{1}$$

$$dNBR2 = NBR2\,(t_1) - NBR2\,(t_2) \tag{2}$$

$$dMIRBI = MIRBI\,(t_2) - MIRBI\,(t_1) \tag{3}$$

where t_2 is the current time, and t_1 is the previous time. Positive values of *dNBR*, *dNBR2,* and *dMIRBI* indicate the presence of a BA, because fire implies a decrease of *NBR* and *NBR*2 and an increase of *MIRBI*. Data at time t_1 contain, for each pixel, the most recent information about the BTSIs. The S2 revisit frequency is 5 days, so, by default, $t_1 = t_2{-}5$. However, if at $t_2{-}5$ a pixel was labelled as cloudy by the SCL map included in each S2 L2A product, the previous values of the indices are maintained. A limit of 30 days is fixed for $t_2 - t_1$ to avoid comparing data acquired at very different times [33].

Change detection is performed in two phases. In the first phase, a clustering algorithm (namely the ISODATA) is applied to the BTSIs to produce a first guess BA (FGBA) map [see Fig. 1(b)]. The maximum number of clusters is 10 and the objects belonging to the cluster presenting the highest median of the pixel values of the BTSIs [red in Fig. 1(b)] are classified as FGBA. A cleanup process consisting of the aggregation of

smaller, adjacent objects regions to a larger object is performed to avoid the presence of many small objects.

A more accurate identification of the BA is carried out through parametric thresholding. The latter might be time consuming, because it requires the estimation of two distribution functions, one representing the BA and the other one the background [27]. Then, AUTOBAM makes a joint use of edge filtering (namely the Roberts filter) and buffering to reduce the number of input pixels for the thresholding to those placed near to the BA-background boundary, thus speeding up the estimation. The Roberts filter is applied to delineate the boundary of the FGBA [see Fig. 1(c)]. Then, a buffer zone around the edge is created [cyan in Fig. 1(d)]. It partially covers both the FGBA and the background. If the FGBA actually corresponds to a BA, the distribution of the pixel values in the buffer is likely bimodal [see Fig. 1(e)]. This is verified by computing the Ashman's D coefficient and the ratio between the modes (R). If D and R are larger than two empirical values found in the literature (2 and 0.2, respectively), the histogram is assumed as bimodal and the Otsu automatic method proposed in [32] is applied to determine the threshold [red line in Fig. 1(e)].

The RGA is adopted to account for the spatial context. The seed region of the RGA is the intersection of the regions identified by applying, for each BTSI, the threshold computed through the Otsu method. A further constraint is that the seed region should be included in the FGBA. For each BTSI, the seed region grows until the edge of the FGBA is reached, but neighboring pixels are added only if their value is larger than a tolerance. To determine the tolerance and to estimate D and R, the bimodal histogram is fitted by two Gaussian functions. Denoted as m the mean value (i.e., the mode) of the function fitting the histogram corresponding to the BA and with s the standard deviation, the tolerance is set to m–2s. The regions generated by the application of the RGA to each BTSI are intersected to derive the final BA. Active fire detections are used to associate a set of quality flags to each BA object.

The AUTOBAM-derived maps have a spatial resolution of 20 m, that is the same of the S2 SWIR bands, which are used in the computation of all the BTSIs. Since NBR also uses the 10 m NIR band, the latter is downsampled to 20 m.

D. Relationships and Matching Between Objects

Performing the validation of a set of mapped BA objects implies verifying whether it is possible to match a mapped object M to a reference object R. If so, the following four new objects can be defined, as described in [23] and schematized in Fig. 2.

1) The intersection object, $M \cap R$, i.e., the area of overlap between M and R, which corresponds to the area correctly classified.
2) The $M \cap \neg R$ object, which corresponds to the commission error.
3) The $\neg M \cap R$ object, which corresponds to the omission error.
4) The union object, $M \cup R$, which is given by: $M \cap \neg R + \neg M \cap R + M \cap R$.

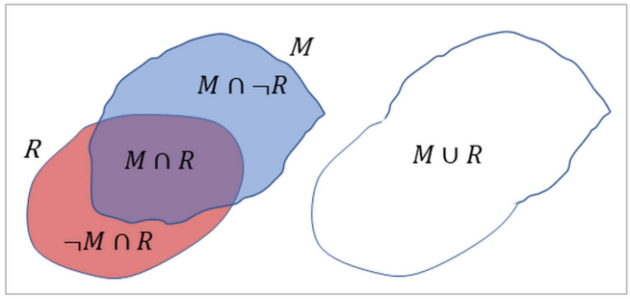

Fig. 2. New objects derived by associating a reference object R (light red) to a mapped object M (light blue).

When validating an S2-derived BA product using ground measurements, the object matching is quite complex. For the present study, the situation is shown in Fig. 3. There is a set of reference objects [see Fig. 3(a)] and a set of mapped objects [see Fig. 3(b)]. First, the number of reference objects is generally different from the number of mapped objects. Moreover, reference objects are identified by a fire date, while mapped ones are identified by the acquisition day of the S2 image through which they have been detected, which is generally different from the fire date. In addition, if a BA is partially obscured by clouds, the corresponding map classifies as burned only the cloud free portion of the area. The other portion of the BA is mapped using one of the following S2 images. This implies that a BA can be oversegmented, i.e., divided in (at least) two segments mapped through two different S2 acquisitions. Note that AUTOBAM is not able to avoid this kind of oversegmentation by reconciling the segments, because it is a NRT system for which the information whether adjacent segments are related to the same fire or different ones is not available.

In a situation like that shown in Fig. 3, there is not a one-to-one relationship between a mapped object and a reference object and there is not an objective method to determine which mapped object corresponds to which reference object [17]. Therefore, we had to apply subjective criteria (both temporal and spatial) to perform the association. In particular, a maximum difference of 30 days between the fire date and the acquisition time of the S2 image of the BA was set to match M and R, in agreement with [33], where the median burned area persistence time was estimated to be 29 days. As for the spatial criterion, in the literature the matching is done by applying a threshold concerning the percentage overlay between mapped and reference objects. As discussed in [17], the threshold varies from 5% (e.g., [34]) to 50% (e.g., [35]) over reference or mapped objects. Since a high threshold may cause an inefficient number of qualified objects for thematic accuracy assessment [17], a 20% threshold over both reference and mapped objects was chosen as done in [27], i.e.

$$\frac{M_{ij} \cap R_{ik}}{R_{ik}} > 20\% \text{ AND} \frac{M_{ij} \cap R_{ik}}{M_{ij}} > 20\%. \quad (4)$$

In (4), index k indicates a generic reference object ($k = 1 : n_R$), index j indicates a generic mapped object ($j = 1 : n_M$) and index i indicates a generic pair of matched objects ($i = 1 : n_{\text{Match}}$).

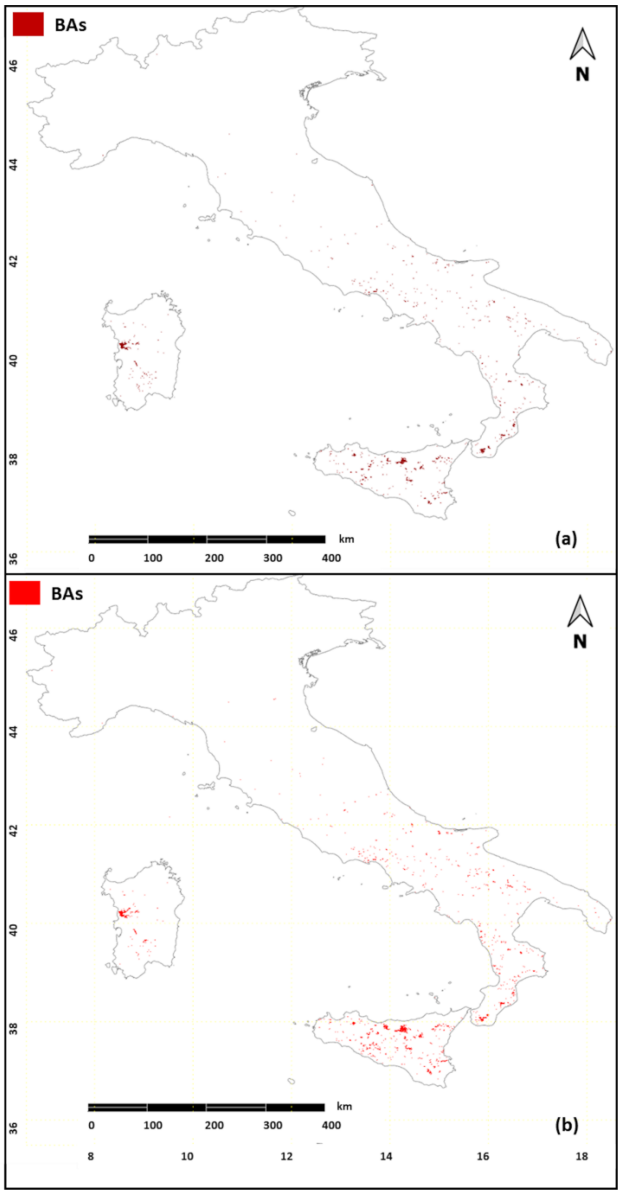

Fig. 3. BAs, for the 2021 fire season, derived (a) from the ground survey and (b) from the daily runs of the AUTOBAM processor.

E. Evaluation of the Segmentation Accuracy

To perform the evaluation of the segmentation accuracy, the entire population of reference data described in Section II-A [see Fig. 3(a)] was considered except for the BAs mainly located in cropland (percentage of cropland pixels larger than 75% [27]). Cropland shows very similar spectral and temporal behavior to BAs and BA discrimination is very difficult or even unfeasible because reflectance changes can be produced by causes different from fires (e.g., anthropic activities like harvesting) [9], [11]. A land cover map derived from the WorldCover product of the European Space Agency [36] was exploited to mask cropland. The WorldCover product has a spatial resolution of 10 m and was derived from Sentinel-2 and Sentinel-1 data. The 2018 Corine land cover layer was also used to further check the accuracy of the masking of cropland. A common reference grid (WGS84 reference ellipsoid, Lat/Lon coordinates, pixel size 20 m) was chosen to reproject the AUTOBAM-derived BA maps and the land cover maps, as well as to rasterize the reference burn polygons. Reference BAs smaller than 1 ha (corresponding to the minimum mapping unit of AUTOBAM [26]) were discarded.

The accuracy metrics reported in Table I, were considered to quantify the following:

1) the similarity in terms of spatial extent, shape and location between matched objects;
2) the object-based thematic accuracy;
3) the global quality of the segmentation.

Most of the metrics were proposed in [23], although metrics proposed in [17], [37] were considered too. In Table I, subscript tot denotes the total area of a set of objects.

For a pair of matched objects (index *i*), the grade of equals s_{11i} and the modified overlap factor s_{31i} quantify the similarity between them, because the higher they are (maximum 1), the more similar the objects are. They have the same numerator, $(M_{ij} \cap R_{ik})$, while the denominator is different, $(M_{ij} \cup R_{ik}$ and $\max(M_{ij}, R_{ik})$, respectively), with s_{31i} that accounts for the proportion between M_{ij} and R_{ik}. The grade of disjoint s_{12i} (basically a complement of s_{11i}), the false positive rate ρ_{fp_i} (related to the commission error), and the false negative rate ρ_{fn_i} (related to the omission error) quantify the dissimilarity between matched objects. The sum of ρ_{fp_i} and ρ_{fn_i} is also known as shape dissimilarity [38].

The location accuracy (LA_i) is based on the Euclidean distance between the centroids of matched objects [23]. In (10), $x_{M_{ij}}$ and $y_{M_{ij}}$ are the coordinates of the centroid of a mapped object M_{ij}, matched with a reference object R_{ik} (whose centroid has coordinates given by $x_{R_{ik}}$ and $y_{R_{ik}}$).

The object-based thematic accuracy was evaluated by computing the completeness *(Compl)* and the correctness *(Corr)* (11)–(12). *Compl* basically corresponds to a per-object user's accuracy because it is determined by dividing the total number of classified objects matched with reference ones (according to (4) in this study) by the total number of classified objects. *Corr* corresponds to a per-object producer's accuracy and is calculated by dividing the total number of classified objects matched with reference ones by the total number of reference objects [35].

The metrics quantifying similarity and dissimilarity can be also applied on overall basis to evaluate the global quality of the segmentation (13)–(17). For this purpose, mapped objects not matched with reference ones and reference objects not matched with mapped ones were considered besides matched objects in order to account for the overall commission and omission errors. Other two parameters were considered to evaluate the global quality. The oversegmentation (*OS*) evaluates the ratio between the total area of overlap between reference and mapped objects with respect to the total area of the reference objects (18). It describes the degree to which an algorithm omits areas which are within the boundaries of the reference object [21]. The undersegmentation (*US*) evaluates the ratio with respect to the total area of the mapped objects (19), thus describing the degree to which an algorithm commits areas which are outside of the boundaries of the reference object [21]. In [17], [37], their root sum square was also used as global metric.

TABLE I
METRICS USED FOR THE EVALUATION OF THE SEGMENTATION ACCURACY

Name	Formula	Range
Mean Grade of Equals	$s_{11m} = \frac{1}{n_{Match}} \sum_{i=1}^{n_{Match}} s_{11i} = \frac{1}{n_{Match}} \sum_{i=1}^{n_{Match}} (M_{ij} \cap R_{ik})/(M_{ij} \cup R_{ik})$ (5)	0-1; optimum: 1
Mean Modified Overlap Factor	$s_{31m} = \frac{1}{n_{Match}} \sum_{i=1}^{n_{Match}} s_{31i} = \frac{1}{n_{Match}} \sum_{i=1}^{n_{Match}} (M_{ij} \cap R_{ik})/\max(M_{ij}, R_{ik})$ (6)	0-1; optimum: 1
Mean Grade of Disjoint	$s_{12m} = \frac{1}{n_{Match}} \sum_{i=1}^{n_{Match}} s_{12i} = \frac{1}{n_{Match}} \sum_{i=1}^{n_{Match}} (\neg M_{ij} \cap R_{ik} + M_{ij} \cap \neg R_{ik})/(M_{ij} \cup R_{ik})$ (7)	0-1; optimum: 0
Mean False Positive Rate	$\rho_{fp\_m} = \frac{1}{n_{Match}} \sum_{i=1}^{n_{Match}} \rho_{fp\_i} = \frac{1}{n_{Match}} \sum_{i=1}^{n_{Match}} (M_{ij} \cap \neg R_{ik})/R_{ik}$ (8)	0-∞; optimum: 0
Mean False Negative Rate	$\rho_{fn\_m} = \frac{1}{n_{Match}} \sum_{i=1}^{n_{Match}} \rho_{fn\_i} = \frac{1}{n_{Match}} \sum_{i=1}^{n_{Match}} (\neg M_{ij} \cap R_{ik})/R_{ik}$ (9)	0-1; optimum: 0
Mean Location Accuracy	$LA_m = \frac{1}{n_{Match}} \sum_{i=1}^{n_{Match}} LA_i = \frac{1}{n_{Match}} \sum_{i=1}^{n_{Match}} \sqrt{(x_{M_{ij}} - x_{R_{ik}})^2 - (y_{M_{ij}} - y_{R_{ik}})^2}$ (10)	0-∞; optimum: 0
Completeness	$Compl = n_{Match}/n_M$ (11)	0-1; optimum: 1
Correctness	$Corr = n_{Match}/n_R$ (12)	0-1; optimum: 1
Overall Grade of Equals (Overall Quality Area)	$s_{11tot} = OQ_a = (M \cap R)_{tot}/(M \cup R)_{tot}$ (13)	0-1; optimum: 1
Overall Modified Overlap Factor	$s_{31tot} = OQ = (M \cap R)_{tot}/max(M_{tot}, R_{tot})$ (14)	0-1; optimum: 1
Overall Grade of Disjoint	$s_{12tot} = [(\neg M \cap R)_{tot} + (M \cap \neg R)_{tot}]/(M \cup R)_{tot}$ (15)	0-1; optimum: 0
Overall False Positive Rate	$\rho_{fp\_tot} = (M \cap \neg R)_{tot}/R_{tot}$ (16)	0-1; optimum: 0
Overall False Negative Rate	$\rho_{fn\_tot} = (\neg M \cap R)_{tot}/R_{tot}$ (17)	0-∞; optimum: 0
Oversegmentation	$OS = 1 - (M \cap R)_{tot}/R_{tot}$ (18)	0-1: optimum 0
Undersegmentation	$US = 1 - (M \cap R)_{tot}/M_{tot}$ (19)	0-1: optimum 0

The flowchart of the procedure applied to compute the metrics listed in Table I is shown in Fig. 4. For each reference object R_k resulting from the rasterization of the reference polygons, the existence of an overlap with mapped objects and the meeting of the conditions expressed by (4) were verified. Then, the extent of the matched objects and of the new objects derived from the matching (see Fig. 2) was computed.

Once the above steps were performed for all the reference objects, *Compl* and *Corr* were calculated (11)–(12). Then, to derive a single value from each metric used to quantify the similarity between matched objects, the mean of s_{11i}, s_{31i}, s_{12i}, ρ_{fp_i}, ρ_{fn_i} and LA_i over the total number of pairs of matched objects (s_{11m}, s_{31m}, s_{12m}, ρ_{fp_m}, ρ_{fn_m}, and LA_m) was computed (5)–(10).

Finally, to derive the global metrics expressed by (13)–(19), the total area of the mapped objects (M_{tot}), the total area of the reference objects (R_{tot}), the total area of overlay between reference and mapped objects $(M \cap R)_{\text{tot}}$, the total area of reference and mapped objects $(M \cup R)_{\text{tot}}$, the total area of mapped objects outside the boundaries of the reference ones $(M \cap \neg R)_{\text{tot}}$ and the total area of reference objects outside the boundaries of the mapped ones $(\neg M \cap R)_{\text{tot}}$ were evaluated.

III. RESULTS

Table II reports, in the second row, the values of the metrics listed in Table I that were obtained by applying the procedure schematized in Fig. 4 to the AUTOBAM outputs (*M*) produced throughout the 2021 fire season (June 1–September 30) and to

TABLE II
VALUES OF THE METRICS LISTED IN TABLE I FOR THE AUTOBAM PRODUCT

s_{11m}	s_{31m}	s_{12m}	ρ_{fp_m}	ρ_{fn_m}	LA_m	$Compl$	$Corr$	s_{11tot}	s_{31tot}	s_{12tot}	ρ_{fp_tot}	ρ_{fn_tot}	OS	US
0.65	0.68	0.35	0.28	0.24	80.5 m	0.67	0.80	0.56	0.72	0.44	0.43	0.25	0.15	0.28
0.74	0.77	0.26	0.14	0.18	55.9 m	0.53	0.63	0.56	0.72	0.44	0.43	0.25	0.15	0.28

Note: Second Row: Threshold=20%; Third Row: Threshold=50%.

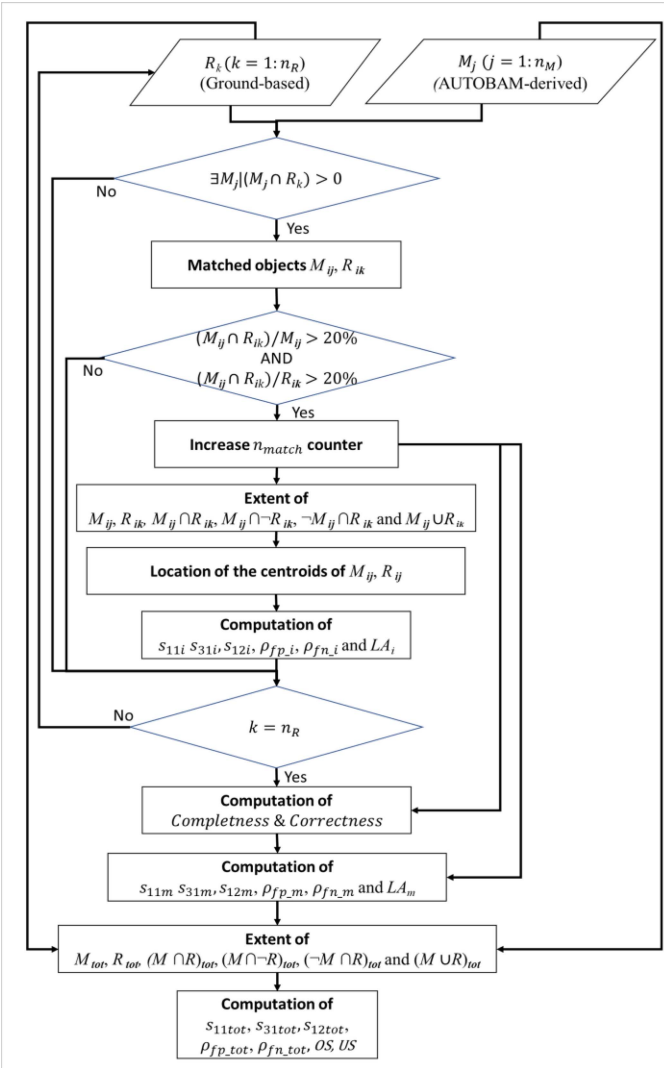

Fig. 4. Flowchart of the procedure applied to compute the metrics listed in Table I.

the ground-based burn polygons used as reference data (R, see Section II-A).

A. Matched/Unmatched Objects

The values of s_{11m} and s_{31m} reported in the second row of Table II indicate that, when an AUTOBAM-derived object was matched to a reference one according to (4), the similarity was quite high, especially in terms of the modified overlap factor ($s_{31m} = 0.68$). The mean area of the intersection between matched objects (i.e., the mean value of $(M_{ij} \cap R_{ik})$) was 46.7 ha.

As for the dissimilarity measures derived considering matched objects, good performances were obtained in terms of both commission and omission errors ($\rho_{fp\_m} = 0.28$, $\rho_{fn\_m} = 0.24$). It is worth noting that the medium grade of disjoint s_{12m} does not actually provide additional information, because it is equal to $1-s_{11m}$. It was included in the list of the accuracy measures for comprehensiveness of information.

TABLE III
VALUES OF THE METRICS LISTED IN (5)–(10) FOR THE EFFIS PRODUCT

s_{11m}	s_{31m}	s_{12m}	ρ_{fp_m}	ρ_{fn_m}	LA_m
0.63	0.68	0.37	0.45	0.19	88.0 m

Note: Threshold=20%

Regarding the object-based thematic accuracy, 1365 reference objects out of 1713 were matched by the (AUTOBAM-derived) mapped ones, corresponding to a *Corr* value equal to 0.80. Note that, because of the exclusion of objects mainly located in cropland, a smaller number of reference objects with respect to [27], was considered in the present study. The total number of mapped objects was 2031, corresponding to a *Compl* value equal to 0.67. Then, although a nonrestrictive value for the threshold adopted to consider a mapped object as matching a reference one (hereafter indicated as matching threshold) was chosen, a quite large number of unmatched mapped objects ($2031-1365 = 666$), was present. These objects were assumed as false positives and the main reason of their presence will be discussed in Section IV.

We also quantified the variations of the values of the accuracy measures due to an increase to 50% of the matching threshold. They are reported in the third row of Table II. As expected, *Corr* and *Compl* decreased to 0.63 and 0.53, respectively, because of the smaller number of matched objects. On the other hand, due to the larger agreement between the remaining objects, s_{11m} and s_{31m} increased (0.74 and 0.77, respectively) and ρ_{fp_m} and ρ_{fn_m} decreased (0.14 and 0.18, respectively).

To show the generality of the proposed validation procedure, we also carried out an exercise using the BAs that were mapped in Italy by EFFIS between June 1, 2021 and September 30, 2021. Since EFFIS was designed to map forest fires larger than 30 ha and the reference dataset also included small fires occurring in other land cover types like shrubland, only matched objects were considered, i.e., only metrics (5)–(10) were computed in this case. The result of this exercise is reported in Table III. The EFFIS product showed a good performance in terms of similarity between matched objects. As for the dissimilarity, a low value of ρ_{fn_m} (0.18) was obtained, while ρ_{fp_m} was much higher (0.45).

B. Global Quality of the Segmentation

As discussed in Section II-E, both the similarity and the dissimilarity measures were calculated not only as a mean, but

also as an overall total area, in order to assess the global quality of the segmentation. Note that, in this case, both matched and unmatched BAs were taken into account, and the results were not affected by the value of the matching threshold.

The total area covered by reference objects (R_{tot}) was ∼85200 ha, while the total area covered by mapped objects (M_{tot}) was ∼100190 ha. The union between M_{tot} and R_{tot}, i.e., $(M \cup R)_{\text{tot}}$, was ∼130290 ha; of that area, 56%, corresponding to ∼72490 ha, was the intersection between M_{tot} and R_{tot}, i.e., $(M \cap R)_{\text{tot}}$ ($s_{11\text{tot}} = 0.56$). A much higher value (0.72) was obtained for $s_{31\text{tot}}$, which, in this case, was equal to the ratio between $(M \cap R)_{\text{tot}}$ and M_{tot}. The large difference between $s_{31\text{tot}}$ and $s_{11\text{tot}}$ shows that they provide different information.

Regarding the metrics related to the commission error, $(M \cap \neg R)_{\text{tot}}$ was ∼36390 ha, corresponding to an overall false positive rate ($\rho_{fp_{\text{tot}}}$) equal to 0.43. This rate was mainly related to mapped objects not matched with reference ones, as discussed in Section IV. *US* did not add significant information being equal to $1 - s_{31\text{tot}}$ in this case, because M_{tot} was larger than R_{tot}. Like s_{12m}, also *US* was included in the list of the accuracy measures for comprehensiveness of information. AUTOBAM gave better results for the measures related to the omission error; $(\neg M \cap R)_{\text{tot}}$ was ∼21400 ha and $\rho_{fn_{\text{tot}}}$ was equal to 0.25. Even the value of *OS* was quite low (0.15).

IV. Discussion

A set of accuracy metrics was computed to perform an object-based validation of a BA product like the AUTOBAM-derived one to provide users with a comprehensive information about its strengths and weaknesses. Although the evaluation of a product based on several accuracy metrics could be difficult for end users, who might require a limited set of scores (such as omission and commission error and/or the Dice coefficient derived from a confusion matrix), we believe that they need to know the following:

1) the number of BA objects that are correctly detected;
2) if and to what extent the spatial extent and the location of actual BA objects are correctly identified (this is particularly important for a moderate resolution BA product);
3) the capability to estimate the total surface that was burned during a fire season.

Regarding point (1), end users may want to use a BA product to derive statistics about the number of wildfires that broke out during a fire season. A reference dataset such as that considered in this study allowed us to perform a reliable counting of this number. We computed not only the percentage of reference objects that were correctly detected *(Corr)*, but also the percentage of the matched objects with respect to the total number of mapped objects *(Compl)*, in order to add the information about the mapped objects that had no correspondence with real-world objects. AUTOBAM gave good results in terms of *Corr*, while worse results were obtained for *Compl* because of the presence of several unmatched mapped objects, as discussed subsequently.

Point (2) is related to the geometric accuracy of matched objects, which is important if the BA product is employed to establish constraints on the land use of the areas affected by fires. This information was provided by the mean values of the accuracy metrics computed for each pair of matched objects. AUTOBAM showed very good performances in terms of dissimilarity (mean false positive and negative rates not exceeding 0.28) and quite good performances in terms of similarity. Then, similarity and dissimilarity measures did not provide redundant information except for s_{11} and s_{12}.The results obtained using a 20% matching threshold indicate that it represented a good compromise between the need to have a quite large number of matched objects for assessing the accuracy of satellite derived BAs and the need to avoid the association between dissimilar objects. This affirmation is corroborated by the low value obtained for another metric related to the geometric accuracy, that is the mean location accuracy (LA_m ∼80 m).

To at least partially tackle the problem of the sensitivity to the matching threshold of the results of the object-based validation, we proposed to compute the mean values of the per-object measures also considering a more restrictive threshold with respect to that selected to perform the whole validation exercise. It must be underlined again that there is not an objective method to determine if a mapped object corresponds to a reference object. We made a nonrestrictive choice for the matching threshold also considering possible inaccuracies in the reference polygons, despite of the metric accuracy of the GPS devices generally used when ground surveys are performed. The delineation of a burn perimeter is to some extent subjective because its definition could be difficult when on the ground. For instance, ground-based mapping of a fire could be difficult because of the challenges of following burned edges in rough terrain and the nonuniform manner in which fires burn across the landscape [22]. On the other hand, as underlined in the Introduction, ground-based polygons can be very useful to validate BA products derived from moderate resolution satellite data.

Point (3) concerns the global quality of the segmentation. In this case, the overall commission and omission errors were taken into account, so that ρ_{fp_tot} was significantly larger than ρ_{fp_m}. The quite high value of ρ_{fp_tot} represented the major weakness of the AUTOBAM processor that overestimated the total surface that was burned during the 2021 fire season. The overestimation was due to the presence of a quite large number of unmatched mapped objects that affected *Compl* too, as previously mentioned. This presence was on its turn mainly due to clouds and cloud shadows that were not (or only partially) detected by the SCL included in the level 2A S2 products. Note that AUTOBAM processes all the available S2 images of Italy, with the only constraint that the overall cloud cover must be less than 40% [26]. Moreover, as underlined in Section II-C, it does not take advantage of the temporal persistence of the BA signal, because of its NRT requirement. Therefore, AUTOBAM cannot verify whether changes in the values of the spectral indices depend on the presence of undetected clouds.

The quite low values of ρ_{fn_tot} and *OS* were consistent with the low number of reference objects not matched with mapped ones with respect to the total number of reference objects. This outcome indicated that AUTOBAM was able to capture the real-world BA objects and limit the omission of areas which are within the boundaries of the reference objects.

Finally, it must be underlined that the proposed procedure is fully automatic, except for the choice of the matching threshold. It can in principle be applied to any country level BA product, because it only requires a reference dataset and a set of classified BA objects derived from satellite data that should be projected on a common geographic grid. We did an experiment using the EFFIS product instead of the AUTOBAM one to highlight this characteristic. The experiment demonstrated that even the EFFIS product showed a good geometric accuracy, even if the use of coarse resolution MODIS data prevented an accurate delineation of small BAs resulting in a quite high value of ρ_{fp_m}.

IV. Conclusion

The quality of a burned area product derived from satellite data is generally evaluated through the confusion matrix. However, end users may also need to know if and how well mapped objects spatially match real-world objects, especially if the product is not derived from coarse resolution (250–500 m) satellite data, but rather from higher resolution (10–20 m) ones. Therefore, this study proposed to complement the validation based on the confusion matrix with a new validation method based on the analysis of the match/mismatch between mapped objects and real-world objects. The analysis was performed at country level (Italy), using as real-world (reference) objects a set of ground-based burn polygons mapped by local authorities. This set represented an independent database, particularly useful when moderate resolution data are used to map burned areas, because, in this case, higher resolution reference data can be difficult to obtain. Mapped objects were mainly generated from Sentinel-2 multispectral data using the AUTOBAM processor. To highlight that the proposed validation method can be applied to any BA product to assess its performances and find out the possible reasons for the dissimilarity with respect to reference data, an experiment on the EFFIS burned area product was carried out too.

By implementing a comprehensive set of accuracy metrics, the strengths and weaknesses of the AUTOBAM BA product were assessed considering both matched BA objects and all the objects. It emerged that AUTOBAM was able to identify actual BA objects with a good geometric accuracy (location and spatial extent), but it tended to produce false positives being not able to mitigate the problem of an inaccurate masking of clouds, mainly because of its near-real time requirement. Even the EFFIS product presented a good accuracy, although only matched objects were analyzed.

The problem of the subjectivity of the choice of the threshold adopted to consider a mapped object as matching a reference one was also pointed out. On one hand, we explained why we selected a nonconservative threshold. On the other hand, the impact of the use of a more restrictive threshold was (at least partially) evaluated.

The object-based validation of the AUTOBAM-derived product using ground-based burn polygons will continue for the fire seasons after 2021. In this way, a more reliable assessment of the product will be performed, and the burned area mapping algorithm will be possibly refined.

References

[1] L. Giglio, L. Boschetti, D. P. Roy, M. L. Humber, and C. O. Justice, "The collection 6 MODIS burned area mapping algorithm and product," *Remote Sens. Environ.*, vol. 217, pp. 72–85, 2018.

[2] J. Lizundia-Loiola, G. Otón, R. Ramo, and E. Chuvieco, "A spatio-temporal active-fire clustering approach for global burned area mapping at 250 m from MODIS data," *Remote Sens. Environ.*, vol. 236, 2020, Art. no. 111493.

[3] D. P. Roy et al., "Landsat-8 and sentinel-2 burned area mapping - A combined sensor multi-temporal change detection approach," *Remote Sens. Environ.*, vol. 231, no. 7, 2019, Art. no. 111254.

[4] E. Chuvieco et al., "Building a small fire database for Sub-Saharan Africa from sentinel-2 high-resolution images," *Sci. Total Environ.*, vol. 845, Nov. 2022, Art. no. 157139.

[5] J. Eidenshink, B. Schwind, K. Brewer, Z. Zhu, B. Quayle, and S. Howard, "A project for monitoring trends in burn severity," *Fire Ecol.*, vol. 3, no. 1, pp. 3–21, 2007.

[6] L. Boschetti, D. P. Roy, C. O. Justice, and M. L. Humber, "MODIS-Landsat fusion for large area 30m burned area mapping," *Remote Sens. Environ.*, vol. 161, pp. 27–42, 2015.

[7] N. R. R. Goodwin and L. J. J. Collett, "Development of an automated method for mapping fire history captured in Landsat TM and ETM + time series across Queensland, Australia," *Remote Sens. Environ.*, vol. 148, pp. 206–221, May 2014.

[8] Y. E. E. Shimabukuro, J. Miettinen, R. Beuchle, R. C. C. Grecchi, D. Simonetti, and F. Achard, "Estimating burned area in Mato Grosso, Brazil, using an object-based classification method on a systematic sample of medium resolution satellite images," *IEEE J. Sel. Topics Appl. Earth Observ. Remote Sens.*, vol. 8, no. 9, pp. 4502–4508, Sep. 2015.

[9] T. J. Hawbaker et al., "Mapping burned areas using dense time-series of Landsat data," *Remote Sens. Environ.*, vol. 198, pp. 504–522, 2017.

[10] T. J. J. Hawbaker et al., "The Landsat burned area algorithm and products for the conterminous United States," *Remote Sens. Environ.*, vol. 244, no. 4, 2020, Art. no. 111801.

[11] E. Roteta, A. Bastarrika, M. Padilla, T. Storm, and E. Chuvieco, "Development of a sentinel-2 burned area algorithm: Generation of a small fire database for sub-Saharan Africa," *Remote Sens. Environ.*, vol. 222, pp. 1–17, 2019.

[12] M. Franquesa et al., "Development of a standard database of reference sites for validating global burned area products," *Earth Syst. Sci. Data*, vol. 12, no. 4, pp. 3229–3246, Dec. 2020.

[13] M. Franquesa, J. Lizundia-Loiola, S. V. Stehman, and E. Chuvieco, "Using long temporal reference units to assess the spatial accuracy of global satellite-derived burned area products," *Remote Sens. Environ.*, vol. 269, Feb. 2022, Art. no. 112823.

[14] L. Boschetti, S. V. Stehman, and D. P. Roy, "A stratified random sampling design in space and time for regional to global scale burned area product validation," *Remote Sens. Environ.*, vol. 186, pp. 465–478, Dec. 2016.

[15] L. Boschetti, D. P. Roy, and C. O. Justice, "International global burned area satellite product validation protocol, Part I—Production and standardization validation reference data," 2009, pp. 1–11.

[16] D. Stroppiana et al., "Sentinel-2 sampling design and reference fire perimeters to assess accuracy of burned area products over Sub-Saharan Africa for the year 2019," *ISPRS J. Photogrammetry Remote Sens.*, vol. 191, pp. 223–234, Sep. 2022.

[17] S. Ye, R. G. Pontius, and R. Rakshit, "A review of accuracy assessment for object-based image analysis: From per-pixel to per-polygon approaches," *ISPRS J. Photogrammetry Remote Sens.*, vol. 141, pp. 137–147, Jul. 2018.

[18] L. Boschetti, D. P. Roy, L. Giglio, H. Huang, M. Zubkova, and M. L. Humber, "Global validation of the collection 6 MODIS burned area product," *Remote Sens. Environ.*, vol. 235, no. 11, 2019, Art. no. 111490.

[19] M. Padilla et al., "Comparing the accuracies of remote sensing global burned area products using stratified random sampling and estimation," *Remote Sens. Environ.*, vol. 160, pp. 114–121, 2015.

[20] R. G. Congalton and K. Green, *Assessing the Accuracy of Remotely Sensed Data*. Boca Raton, FL, USA: CRC Press, 2008.

[21] M. L. Humber, L. Boschetti, and L. Giglio, "Assessing the shape accuracy of coarse resolution burned area identifications," *IEEE Trans. Geosci. Remote Sens.*, vol. 58, no. 3, pp. 1516–1526, Mar. 2020.

[22] C. A. Kolden and P. J. Weisberg, "Assessing accuracy of manually-mapped wildfire perimeters in topographically dissected areas," *Fire Ecol.*, vol. 3, no. 1, pp. 22–31, 2007.
[23] T. G. Whiteside, S. W. Maier, and G. S. Boggs, "Area-based and location-based validation of classified image objects," *Int. J. Appl. Earth Observation Geoinf.*, vol. 28, no. 1, pp. 117–130, 2014.
[24] T. Blaschke et al., "Geographic object-based image analysis - towards a new paradigm," *ISPRS J. Photogrammetry Remote Sens.*, vol. 87, pp. 180–191, Jan. 2014.
[25] M. Baatz, C. Hoffmann, and G. Willhauck, "Progressing from object-based to object-oriented image analysis," *Lecture Notes Geoinf. Cartogr.*, vol. 1, no. 9783540770572, pp. 29–42, 2008.
[26] L. Pulvirenti et al., "An automatic processing chain for near real-time mapping of burned forest areas using sentinel-2 data," *Remote Sens.*, vol. 12, 2020, Art. no. 674.
[27] L. Pulvirenti, G. Squicciarino, E. Fiori, D. Negro, A. Gollini, and S. Puca, "Near real-time generation of a country-level burned area database for Italy from sentinel-2 data and active fire detections," *Remote Sens. Appl. Soc. Environ.*, vol. 29, 2023, Art. no. 100925.
[28] J. M. P. Nogueira, J. Ruffault, E. Chuvieco, and F. Mouillot, "Can we go beyond burned area in the assessment of global remote sensing products with fire patch metrics?," *Remote Sens.*, vol. 9, no. 1, 2017, Art. no. 25025.
[29] M. K. Vanderhoof, T. J. Hawbaker, C. Teske, A. Ku, J. Noble, and J. Picotte, "Mapping wetland burned area from Sentinel-2 across the southeastern United States and its contributions relative to Landsat-8 (2016–2019)," *Fire*, vol. 4, no. 3, 2021, Art. no. 25142.
[30] M. Boschetti, D. Stroppiana, and P. A. Brivio, "Mapping burned areas in a Mediterranean environment using soft integration of spectral indices from high-resolution satellite images," *Earth Interact.*, vol. 14, no. 17, pp. 1–20, 2010.
[31] J. San-Miguel-Ayanz, E. Schulte, G. Schmuck, and A. Camia, "The European Forest Fire Information System in the context of environmental policies of the European Union," *Forest Policy Econ.*, vol. 29, pp. 19–25, Apr. 2013.
[32] N. Otsu, "A threshold selection method from gray level histograms," *IEEE Trans. Syst., Man, Cybern.*, vol. 9, no. 1, pp. 62–66, Jan. 1979.
[33] A. Melchiorre and L. Boschetti, "Global analysis of burned area persistence time with MODIS data," *Remote Sens.*, vol. 10, no. 5, 2018, Art. no. 20142.
[34] D. G. Leckie, F. A. Gougeon, S. Tinis, T. Nelson, C. N. Burnett, and D. Paradine, "Automated tree recognition in old growth conifer stands with high resolution digital imagery," *Remote Sens. Environ.*, vol. 94, no. 3, pp. 311–326, Feb. 2005.
[35] Q. Zhan, M. Molenaar, K. Tempfli, and W. Shi, "Quality assessment for geo-spatial objects derived from remotely sensed data," *Int. J. Remote Sens.*, vol. 26, no. 14, pp. 2953–2974, 2005.
[36] D. Zanaga et al., "ESA WorldCover 10 m 2020 v100 (version v100)," *Dataset*, Oct. 20, 2021. Accessed: Mar. 31, 2023. [Online]. Available: https://zenodo.org/record/5571936
[37] M. Belgiu and L. Drăguţ, "Comparing supervised and unsupervised multiresolution segmentation approaches for extracting buildings from very high resolution imagery," *ISPRS J. Photogrammetry Remote Sens.*, vol. 96, pp. 67–75, Oct. 2014.
[38] U. Weidner, "Contribution to the assessment of segmentation quality for remote sensing applications," *Int. Arch. Photogrammetry, Remote Sens. Spatial Inf. Sci.*, vol. 37, no. B7, pp. 479–484, 2008.

Luca Pulvirenti (Member, IEEE) received the Laurea degree in electronic engineering and the Ph.D. degree in electromagnetism from the Sapienza University of Rome, Rome, Italy, in 1999 and 2004, respectively.

He was a Postdoctoral Researcher with the Department of Electronic Engineering, Sapienza University of Rome, from 2004 to 2009 and a Fixed-Term Researcher with the Department of Information Engineering, Electronics and Telecommunications, Sapienza University of Rome, from 2010 to 2013. Since 2013, he has been a Researcher with CIMA Research Foundation, Savona, Italy, where he is currently the Head of the Earth Observation unit. His research interests include remote sensing of the Earth's surface, with particular emphasis on hydrological applications of remote sensing and the development of processors for mapping the extent of disasters like floods and forest fires using remote sensing data. He was involved in several projects, funded by national and international institution, on the use of Earth Observation data for hydro-meteorological risk management. He has authored/coauthored more than 50 publications on peer-reviewed journals.

Dr. Pulvirenti is a member of the Italian Association of Remote Sensing.

Giuseppe Squicciarino received the Laurea degree in environmental engineering from the Basilicata University, Potenza, Italy, in 2003.

From 2003 to 2006, he was a Research Consultant with the Environmental Engineering and Physics Department, University of Basilicata, for monitoring activities on desertification risk assessment, in the Basilicata region, and meteorological data collection and processing for hydrological model calibration. From 2006 to 2008 he was doing research in CIMA and, from 2009, in CIMA Foundation on data procurement and processing for civil protection applications, especially flood events, with particular emphasis to Cosmo-SkyMed constellation's images. Since 2015, he was also involved in the implementation of models and instruments for analysis of environmental risks produced by natural phenomena, especially related to flood hazard, and evaluation of the damage occurred to exposed elements. Since 2020, he has been a member of the Earth Observation Unit in Cima Foundation and his main activities concern satellite image processing chains, including various type of EO data, finalized to the generation of added value products for flood and fire events.

Dario Negro received the Laurea degree in environmental science from the Salento University, Lecce, Italy, in 2003.

He is a national civil protection Officer. Since 2004 he has attempted many training courses inside the European Civil protection mechanism. His current research interests include planning and prevention activities against wildfires at strategical level. Since 2004 he has been supporting the implementation and test for the operative application of satellite technologies in support to wildfires activities. He is involved as wildfires expert in several national and international projects.

Silvia Puca received the Laurea degree in mathematics from the Sapienza University of Rome, Rome, Italy, in 1999. She has been the Project Manager of the "EUMETSAT Satellite Application Facility on Support to Operational Hydrology and Water Management (H-SAF)" since 2022 and a member of the NASA Precipitation Measurement Mission Science Team since 2013. She works with the Natural Risk Management Office, Italian Civil Protection Department, Rome, Italy. She is alternate national delegate at the Space Surveillance and Tracking Commission's Expert Group of the European Commission. She collaborated with Word Food Programme as "risk mapping and assessment" and "early warning system" expert to develop guidelines on the use of satellite data for the monitoring of meteorological severe events.